Advances in Water Resources 43 (2012) 52–66

Contents lists available at SciVerse ScienceDirect

Advances in Water Resources

journal homepage: www.elsevier.com/locate/advwatres

Towards closure relations in the Representative Elementary Watershed (REW) framework containing observable parameters: Relations for Hortonian overland flow

E. Vannametee *, D. Karssenberg, M.F.P. Bierkens

Department of Physical Geography, Faculty of Geosciences, Utrecht University, P.O. Box 80115, 3508TC Utrecht, The Netherlands

ARTICLE INFO

Article history:
Received 23 December 2011
Received in revised form 8 March 2012
Accepted 30 March 2012
Available online 10 April 2012

Keywords:
Representative Elementary Watershed
Closure relations
Lumped model
Infiltration
Hortonain overland flow
Synthetic hydrologic-response data set

ABSTRACT

This study presents the derivation procedure of an integrated closure relation for infiltration and Hortonian overland flow in the Representative Elementary Watershed (REW) framework that contains directly-observable parameters. A physically-based high resolution model is used to simulate the infiltration flux and discharge for 6×10^5 set of synthetic REWs and rainstorms scenarios. This synthetic data set serves as a surrogate of real-world data to deduce the closure relation. The closure relation performance is evaluated against the results from the high resolution model. The results show that the closure relation is capable of predicting accurate hydrological responses for an independent set of synthetic REWs and rainstroms in terms of the Nash–Sutcliffe index, errors in total discharge volume, and peak discharge, especially in cases where a relatively large amount of runoff is produced with fast responses. For the estimation of parameters in the closure relation, a local method using inverse distance weighted interpolation in the parameter space is superior to the global method based on the multiple regression, resulting in a better reproduction of runoff characteristics.

© 2012 Elsevier Ltd. All rights reserved.

1. Introduction

Conceptual watershed models consider the watershed as a set of interconnected, conceptual, mostly lumped, storages. Small-scale variabilities within the watershed are not explicitly taken into account as they are lumped in the equations and parameters. As a result, the number of parameters is small, which is advantageous during calibration as it minimizes the problem of equifinality [1]. In addition, model run times will be short which allows the use of computationally intensive calibration schemes or application of the model at continental scales. A notable disadvantage of most conceptual watershed models however is that they are not rooted in physics. As a result, the parameters do not have a physical meaning and cannot be estimated unambiguously from observations.

A framework that overcomes this problem is the Representative Elementary Watershed (REW) approach which provides physically-based equations for a watershed as a whole (i.e. lumped model) [2,3]. A REW is divided into sub-zones, each representing a particular hydrological compartment with associated processes [2,4–6]. The balance of mass, energy and momentum within the individual sub-zones of the REW are described by a set of physically-based equations derived from thermodynamic principles by means of averaging over the sub-zones in space and time. Thus, the REW approach presents, potentially, a novel framework for developing, in a comprehensive manner, physically-based watershed models directly applicable at the catchment scale [2].

In REW approach, explicit quantification of the mass flux terms used in the balance equations is required for each REW sub-zone. The cross-boundary fluxes between REW sub-zones must be specified by functional relationships between state and system attributes, referred to as closure relations [6–8]. A key to success in the REW approach is the proper identification of these closure relations [6–14]. It turns out that for successful identification and application of closure relations, three issues are of particular importance.

One is the representation of sub-REW scale spatial heterogeneities of catchment attributes and processes. Although the REW framework itself is scale independent, i.e. it applies to any size of watershed as long as all REW zones are included, a number of closure relations are shown to be dependent on the size and geometry of REWs. This is because the effect of sub-REW scale spatial heterogeneities on the closure relations may change with size and geometry, such as the spatial heterogeneity of surface topography. The evapotranspiration flux, for instance, depends on incoming solar radiation, which is a function of the topography within the REW. This is noted in the study of Mou et al. [13] although they left it for future research to identify the effect of topography. Another example is the saturated area fraction, which depends also on

* Corresponding author. Tel.: +31 302532183.
E-mail address: e.vannametee@uu.nl (E. Vannametee).

0309-1708/$ - see front matter © 2012 Elsevier Ltd. All rights reserved.
http://dx.doi.org/10.1016/j.advwatres.2012.03.029

sub-REW topography, as shown by Lee et al. [8] who use TOPMODEL and sub-REW topography to estimate this fraction. Also, infiltration fluxes are dependent on hillslope length, width, and micro relief [8,15]. The lateral subsurface flux to the channel zone is controlled by plan shape, profile curvature and variation in soil depth over the hillslope domain [16–18].

The second issue is how boundary conditions (inputs) as well as storage of REW zones are used in the calculation of fluxes at boundaries. Most current approaches derive cross-boundary fluxes from the current storage of zones. The study by Beven [7], indicates that past trajectories of storage may need to be considered as well, in order to represent hysteresis. In addition, boundary conditions may change the form of (or parameters in) the closure relations. This seems to be of particular importance for closure relations for infiltration and overland flow, as these processes depend on rainfall intensity [8,15]. Therefore, boundary conditions should be included in the closure relations.

Most important for the application of the REW approach to real catchments, however, is the issue of model parameter identification. Direct estimation of parameter values at the support of the REWs is difficult or impossible with existing field techniques, as these mostly provide representative parameter values at the point to plot scale. Also, many closure relations require scaling parameters to represent the abovementioned sub-REW scale spatial heterogeneities [4,6,14]. As these scaling parameters are in essence conceptual, they cannot be measured directly by definition. Due to the problem with direct estimation of parameter values from field measurements, application of REW models to real catchments requires calibration of model parameters (e.g. [10,13,19]). This poses limitations on the application of the REW concept to ungauged catchments.

Taking these issues into account, we hypothesize that the closure relation C of a zone can be written as $e_t = C(\boldsymbol{i_t}, \boldsymbol{s_t}, \boldsymbol{p}, \boldsymbol{u})$ with e_t the cross-boundary flux at time t; $\mathbf{i}_t$ the input at time t; and $\mathbf{s}_t$ the storage at time t. These terms are required for a correct mass balance. To avoid the need of calibration, the parameters $\mathbf{p}$, which represent hydrological properties of the REWs, should be observable in the field. In addition, a set of scale-transfer parameters $\mathbf{u}$ are required to account for the effect of sub-REW scale variabilities and hysteresis. It is hypothesized that these can be modeled as $\mathbf{u} = f(\mathbf{g}, \overline{\mathbf{i}_t}, \overline{\mathbf{s}_t}, \mathbf{p})$ with REW geometry $\mathbf{g}$; trajectories of input $\overline{\mathbf{i}_t}$ and storage $\overline{\mathbf{s}_t}$, and sub-REW variability in $\mathbf{p}$. f is identified as a regression-based model in Xu [20] and Yokoo et al. [21]. Although a large number of studies consider the abovementioned relations, albeit mostly outside the context of REW, evaluating these expressions for all effects and zones remains a massive challenge. Therefore, we restrict ourselves to the cross-boundary fluxes related to infiltration-excess (Hortonian) overland flow, i.e. infiltration (e^{uc}) and concentrated overland flow (e^{oc}) [2]. In the previous studies (e.g. [8,10,14,22]), the closure relations for infiltration and overland flow were derived on an individual basis without explicit consideration of the direct effects of REW geometry and interactions between these processes. However, the infiltration process and concentrated overland flow generation mechanism are highly dependent and considerably influenced by the geometry of REWs [15,23–25]. In this study, we propose an integrated closure relation for infiltration and concentrated overland flow that explicitly incorporates the effects of REW geometry in the scaling parameters $\mathbf{u}$. The key research question is how to identify a closure relation C that can be parameterized by a relation f that has observable REW geometry and physical properties as input. This would allow to apply the closure relation to a wide range of REW geometry and rainstorm characteristics without calibration.

To achieve the goal, we address the following questions. First, is it possible to obtain the closure relation that allows the calibration of the scaling parameters $\mathbf{u}$ against the observational data? If so, how the closure relation performs with the calibrated scaling parameters? Due to the problem associated with scarcity and scale incompatibility of observational data, we generate a synthetic data set of rainstorm responses using a high resolution physically-based model for a large set of combinations of rainstorm characteristics and REW geometry. The data set is considered as a surrogate of observational real-world data and is used for identification and parameterization of the closure relation C. Second, we investigate the form of the relation f between the scaling parameters $\mathbf{u}$ and observable properties such as REW geometry, rainstorm characteristics and parameters $\mathbf{p}$. This leads to the investigation on how well the scaling parameters $\mathbf{u}$ in the closure relation can be estimated using this relation compared to those obtained from calibration. Finally, we validate the approach using an independent synthetic data set containing REWs that were not used for identifying C and f.

The paper is structured as follows. The general framework of the approach is given in the first part of the paper. After this, we outline the procedures to develop the closure relation for infiltration and Hortonain overland flow when the closure relation is calibrated directly against the artificial data set (i.e. as a benchmark). Then, we develop methods to derive the scaling parameters $\mathbf{u}$ in the closure relation from observable REW properties and rainstorm characteristics. Finally, the closure relation is validated with a set of independent REWs.

2. General framework

The closure relation for infiltration and concentrated overland flow is developed as a lumped conceptual model. The conceptual model can only be identified and parameterized using observations [26]. However, due to the difficulty of directly observing dynamic internal state variables and integral cross-boundary fluxes [1,27,28], a large data set of mass exchange flux and the states of infiltration and overland flow between sub-zones for an extensive set of REWs does not exist. A solution to this problem is to generate a synthetic artificial data set from the synthetic REWs by virtual experiments using numerical models [29,30]. Recent studies (e.g. [29,31–34]) have shown promising results in using this technique to provide an additional source of hydrologic information for hypothesis testing and model development when data scarcity impedes the accomplishment of these tasks. This technique may provide the clues for the forms of the cross-boundary fluxes that can be parameterized in a relatively simple way, as suggested by Beven [7]. Here, we use a physically-based high-resolution rainfall-runoff model to generate an artificial data set of infiltration and discharge. The model is run for a large number of scenarios (approximately 6×10^5 scenarios) that represent different characteristics of net rain (i.e. the amount of rain after subtraction of water by the interception process), physical properties of REWs (i.e. slope gradient, unit length and regolith properties), antecedent moisture conditions, and flow patterns (Fig. 1).

In the second step, the closure relation C for infiltration and concentrated overland flow at the REW scale is formulated. The closure relation is designed as a lumped conceptual process-based model, consisting of a set of simple equations representing key processes only.

Third, parameters $\mathbf{p}$ and $\mathbf{u}$ in the closure relation are found by calibration of the closure relation against the artificial data set separately, for each scenario of REW geometry and rainstorm characteristics in the data set.

In the final step, we derive the scaling parameters in the closure relation from measurable properties of REWs and rainstorm characteristics (i.e. without calibration to the results from the high resolution model, see Fig. 1). This is done following two approaches

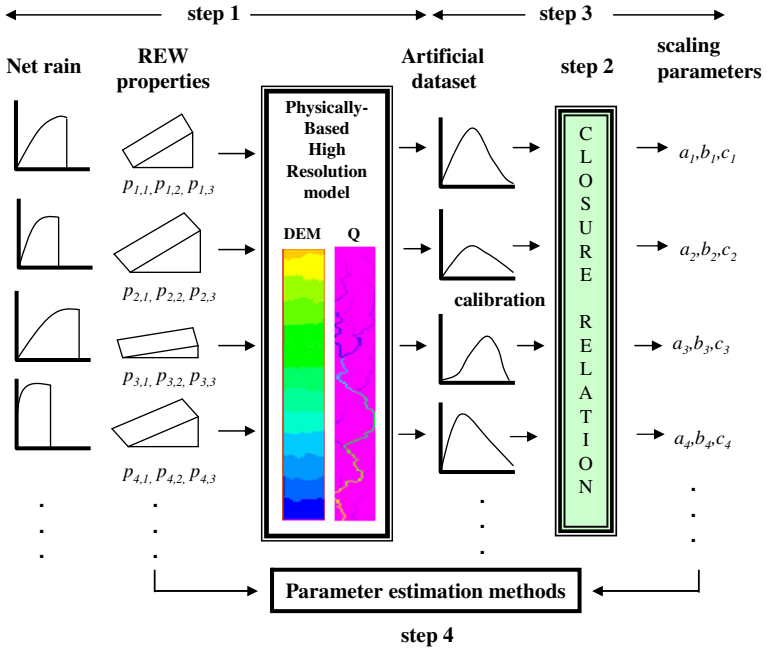

Fig. 1. The development framework of a closure relation for infiltration and Hortonian overland flow. The procedure consists of 4 steps: (1) synthesis of the artificial discharge data set, (2) formulation of the closure relation, (3) parameterization of the closure relation, (4) estimation of the scaling parameters a_i, b_i, c_i in the closure relation from measurable unit properties and rainstorm characteristics for each scenario run i. REW is Representative Elementary Watershed. DEM is digital elevation model. Q is discharge. $p_{i,n}$ are a set of n physical properties of REW of scenario run i in the physically-based high resolution model.

(1) a global method using a multiple regression technique and (2) a local method using an inverse distance weighted interpolation method in the parameter space.

Finally, the closure relation is validated against the results of high resolution model for a set of arbitrarily-defined REWs and rainstorms that have not been used in the identification of the closure relation.

3. Methodology

3.1. Artificial data set

3.1.1. Physically-based high resolution model

A physically-based event-based high resolution model is developed to create the artificial discharge data set. The main runoff generating mechanism of the high resolution model is infiltration-excess Hortonian overland flow. In principle, it is preferable to use a completely physically-based model (e.g. [35]) with a very fine resolution considering all forms of spatial variability in physical parameters. However, such a model would have large run times, which is not feasible. To deal with this issue, we select relatively simple model equations that still have a physical basis, which are solved at a resolution that results in acceptable run times. The grid cell size of 1 m^2 used here is sufficiently small to assume homogeneity of infiltration processes within a grid cell. Simulation of net rainfall and runoff is done using a time step (Δt, h) of 1/360 h (i.e. 10 s) over a rectangular plane, which is regarded as a REW without runon across its boundaries. The model is built with Python 2.5 with library extensions of PCRaster [36].

The model forcing or driver of the system is the net rain, $R_{net,t}$ (m/h), defined as an event. The physically-based high resolution model takes into account the processes of infiltration, surface depression storage, and surface runoff routing (Fig. 2).

Infiltration is simulated as one-dimensional vertical flow into the soil column. The Green & Ampt infiltration equation for one soil layer under a ponded condition is used because it is one of the simplest physically-based infiltration models that uses measureable point-scale soil parameters. To satisfy the assumptions of the Green & Ampt model, the soil is assumed homogeneous, deep and well-drained with homogenous moisture content over the soil column. The wetting front is formed as a distinct sharp boundary, which separates a zone that has been wetted from a totally unwetted soil. The Green & Ampt equation is [37,38]:

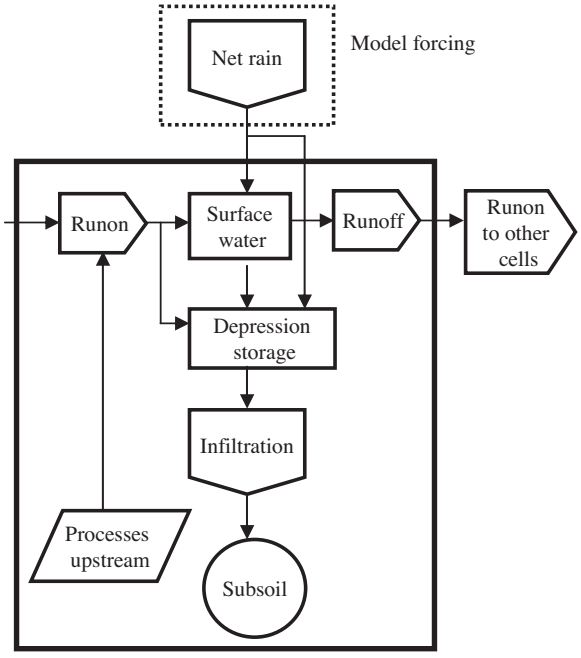

Fig. 2. Schematic of the physically-based high resolution model. The diagram shows processes at a single grid cell.

$$f_{p,t} = K_s\left(1 + \frac{H_f(\eta - \theta_i)}{F_t}\right) \quad (1)$$

where $f_{p,t}$(m/h) is potential infiltration rate at t, K_s (m/h) is saturated hydraulic conductivity, H_f (m) is matric suction at the wetting front, η (−) is soil effective porosity, θ_i (−) is antecedent moisture content, F_t (m) is cumulative infiltration at t. The actual infiltration rate at t, $f_{a,t}$ (m/h), is determined as the smaller value of the potential infiltration rate, $f_{p,t}$, and the water that is available for infiltration over the time step of interest. Under a condition without surface runoff, the amount of water available for infiltration is the depth of water stored in the surface depression storage over the time step of interest. Once surface runoff is generated, the amount of water available for infiltration is:

$$S_t = (R_{net,t} + Q_{on,t}) \cdot \Delta t + S_{ss,t} \quad (2)$$

where S_t (m) is the depth of surface water available in the cell at t, $Q_{on,t}$ (m/h) is the runon flux to the cell at t, $S_{ss,t}$ (m) is the depth of water stored in the depression storage of the cell at t.

The depression storage is water that is temporally retained on the soil surface due to depressions caused by micro relief. Following Onstad [39] and Govers et al. [40], the maximum depth of water that can be stored in the depression storage is:

$$S_{ss,max} = 0.112RR + 0.31RR^2 - 0.012RR \cdot s \quad (3)$$

where $S_{ss,max}$ (mm) is maximum depression storage, RR (mm) is random roughness [41], s is slope gradient (%). The maximum depression storage is used to define a threshold of water that can be stored in a grid cell. Depths of water below this threshold will not become surface runoff. The depression storage receives water from net rain and runon from neighboring upstream cells.

Surface runoff generally occurs in the form of concentrated flow due to the small differences in topography. The Saint–Venant equations of continuity and momentum are used to route surface runoff over the flow network. The kinematic wave theory is suitable to describe the mechanism of overland flow because the slope gradient of units in our study is large. A balance between the friction and gravity forces can be assumed, neglecting the local acceleration, convection acceleration and pressure term in the momentum equation [42,43]. The two-dimensional continuity kinematic wave equation is written as [44]:

$$\frac{\partial A_t}{\partial t} + \frac{\partial Q_t}{\partial x} = R_{net,t} - f_{a,t} \quad (4)$$

where A_t (m^2) is the wet cross sectional area of a pixel at t, Q_t (m^3/h) is runoff at t, x (m) is flow distance. Combining the kinematic wave model with Manning's equation, the relation between the wet cross section of a grid cell and discharge can be expressed as:

$$A_t = \alpha_t Q_t^{\beta} \quad (5)$$

where β is the channel parameter, equal to 0.6 [44]; α_t is:

$$\alpha_t = \left(\frac{n}{\sqrt{S_0}} P_t^{2/3}\right)^{\beta} \quad (6)$$

where P_t (m) is wet perimeter at t, S_0 (−) is slope gradient, n (h/m$^{1/3}$) is Manning roughness coefficient. Surface water is routed downstream over a local drainage direction network, which is computed using the 8-point pour algorithm [45] where each cell drains to its steepest downstream neighbor. The kinematic wave equation is numerically solved for each flow segment on the local drainage direction network by a four-point time-explicit finite-difference solution together with Manning's equation [44] for each simulation time step.

3.1.2. Scenarios to create the artificial data set

The hydrologic responses of the REWs are determined by precipitation and catchment physiographic factors. Therefore, we define the model scenarios based on (1) event characteristics, (2) physical properties of REWs, and (3) antecedent wetness condition.

For the event characteristics, a rainstorm is described by rainfall intensity P_t (m/h), and rainfall duration T (m), assuming constant intensity over the period of a rain event. Interception of rain by vegetation is described by an exponential function using the cumulative precipitation $R_{cum,t}$ (m) [46]:

$$S_{ic,t} = V_{frac} \cdot S_{ic,m} \cdot \left[1 - \exp\left(-k\frac{R_{cum,t}}{S_{ic,m}}\right)\right] \quad (7)$$

Net rainfall $R_{net,t}$ (m/h), which is the temporally-variable amount of water reaching the soil surface after abstraction by vegetation, is calculated as:

$$R_{net,t} = \min\left(R_t - \frac{S_{ic,t} - S_{ic,t-\Delta t}}{\Delta t}, 0\right) \quad (8)$$

where 'min(x,y)' assigns the minimum value of x and y, $S_{ic,t}$ (m) is interception storage, V_{frac} (−) is the fraction of a cell covered by vegetation, $S_{ic,m}$ (m) is canopy storage capacity, k (−) is the extinction factor, $S_{ic,t-\Delta t}$ (m) is the depth of rain water stored in the interception storage at $t - \Delta t$. We assume homogeneous vegetation parameters over REWs, resulting in a uniform interception capacity. Also, interception parameters are not taken variable in creating the scenarios. This is done to limit the number of scenario runs. Note that rainstorm characteristics used in creating the scenarios (i.e. rain intensity and event duration) already provide a large range of different net rain characteristics. The parameter values used in Eq. (7) are given in Table 1.

The properties of REWs include geometric and hydraulic properties. The geometric properties describe the size and shape of REWs as a hillslope section in REWs with the length L (m), a constant slope gradient S_{avg} (m/m), and micro relief z (m). The elevation, H (m), of a cell is:

$$H = S_{avg} \cdot Y + z \quad (9)$$

with, Y (m) the distance from the downstream border. The microrelief is small scale variation of topography which is regarded as a realization of a random variable z, with zero mean and a spatial pattern defined by a circular semivarigram model. Under the assumptions of intrinsic stationary conditions [49], the spatial correlation of micro relief z is defined by

$$\begin{aligned} \gamma(h) &= c_0 + c_1\left(\frac{2h}{\pi a}\sqrt{1 - \left(\frac{h}{a}\right)^2} + \frac{2}{\pi}\arcsin\frac{h}{a}\right); && \text{for } 0 < h < a \\ &= c_0 + c_1; && \text{for } h \geq a \end{aligned} \quad (10)$$

where $\gamma(h)$ is semivariance as a function of separation distance h, c_0 (m) is the nugget, c_1 (m) is the sill variance and a (m) is the correlation range of the semivariogram. The variable c_1 is considered as an independent variable to be used in creating the scenarios while c_0 and a are fixed. This is because the variation of relief height have the largest effect in determining the height difference over the plane. The values of c_0 and a are obtained from the field observations of micro relief. Field observations were collected on an agricultural field in the Buëch catchment, France [50]. The micro relief was measured at a 0.1 m interval over measurement transects of 5 and 10 m. For each measurement transect, the semivarience was calculated and fitted by the circular variogram model. The average values of c_0 and a of all measurement transects are used. Realizations of micro-scale relief are generated following Pebesma and Heuvelink [51]. The micro relief plays a role in determining the flow pattern between the units. If the spatial variance of micro relief (c_1) is small, which means small elevation differences between cells, a parallel flow pattern is generated. If the micro relief has large spatial variance, flow paths more often converge as shown in Fig. 3.

Table 1
Values used to calculate the interception loss[a].

Parameters	Description	Values	Remarks
$S_{ic,m}$	Canopy storage capacity (m)	0.0328	Representative for agricultural area, using the equation proposed by von Hoyningen–Huene [47]
k	Extinction factor (−)	0.23	Representative for agricultural area [48]
V_{frac}	Vegetation cover fraction (−)	0.45	Assumed vegetation cover over almost half of the area of the units (45%)

[a] See Eq. (7).

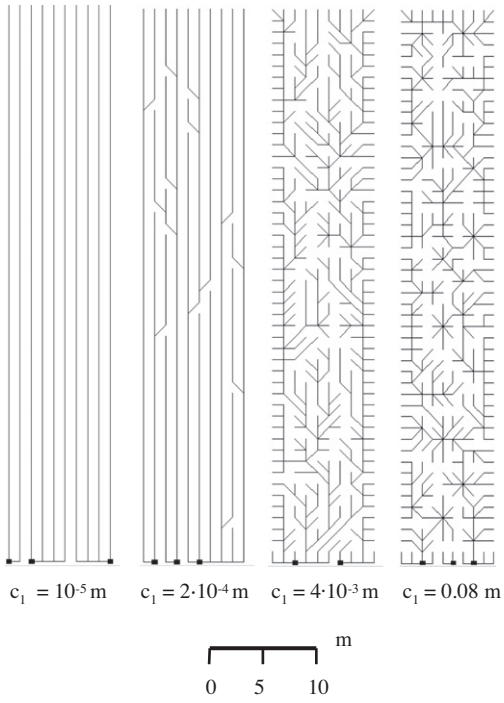

Fig. 3. Examples of flow patterns, generated with different values of c_1. Average slope gradient (S_{avg}) is 0.06. The lines represent flow directions of each cell with a general flow direction from top to bottom in the figure; the black square dots identify cells draining across the boundary of the units. The figure shows only a small part of REW.

Note that variation in topography defined by Eq. (10) is only used for generating the flow pattern but not for calculating the depression storage. The depression storage occurs within a cell, at a shorter scale of variation in topography than the variation that generated the flow pattern.

The hydraulic properties of units govern the infiltration process. These properties are saturated hydraulic conductivity (K_s) and matric suction at the wetting front (H_f). The antecedent wetness condition before a rainstorm is characterized by the soil moisture content (θ_i) of the REW. To keep our problem computationally tractable, we assume uniform soil hydraulic properties over REWs. This is a limitation, but it has been shown by Karssenberg [15] that the effects of spatially non-uniform infiltration parameters on the runoff responses are only pronounced in the case of large variability. Also, the runoff responses from purely-random fields of infiltration parameters may resemble those obtained from the homogeneous case as found by Merz and Bárdossy [52]. Note that, although the soil hydraulic properties are assumed uniform over REWs, Hortonian runoff generation mechanism is considered as a spatial process in the high resolution model. During a storm period, infiltration flux is spatially uniform and runoff is generated over an entire REW. However, after the storm period, infiltration flux becomes spatially variable; and only parts of the REW generate runoff. This is due to the flow pattern and the effect of runon on the runoff generation mechanism.

The scenarios are defined as all possible combinations of a set of model inputs (i.e. event characteristics, properties of REWs and antecedent condition). Four values are chosen as a geometric series for each model input resulting in $4^8 = 65{,}536$ scenarios or model runs (Table 2).

A number of other model inputs is not varied between scenarios because these inputs are considered having smaller effects on the hydrologic responses of the REWs. Fixed values of these inputs are given in Table 3.

The high resolution model is run on an event basis. For each scenario run, the results of the high resolution model (i.e. runoff and state variables) at selected simulation time steps (i.e. each minute) are stored in a database. The discharge database will be used in the identification of closure relation.

3.2. Development of the closure relation for infiltration and concentrated overland flow

The closure relation for infiltration and concentrated overland flow is developed as a lumped conceptual model. The closure relations were built iteratively by adjusting its structure until a satisfactory correspondence of simulated hydrographs and hydrographs in the artificial data set was found, while keeping the model structure as simple as possible. The simulation time step in the lumped model can be different from that used in the high resolution model. The subscript t in the lumped equations used in the closure relation represents time as an index (e.g. $t = 1,2,3,\ldots$). Water stored in the system at the time index t is calculated as the depth of the surface water layer:

$$S_t = S_{t-1} + (R_{net,t} - I_{a,t} - q_t) \tag{11}$$

where S_{t-1} (m) is the depth of surface water at $t-1$, $R_{net,t}$ (m) is net rain at t, $I_{a,t}$ (m) is the actual infiltration depth between $t-1$ and t, q_t (m) is the depth of discharge generated between $t-1$ and t, which is calculated by the discharge generated at the time step of interest divided by the area of REW.

The Green & Ampt model, Eq. (1), is used to describe the potential infiltration in the closure relation. As the infiltration flux in the high-resolution model is not spatially uniform after the rainstorm period due to the runon effects over the flow network, it is required to use a ponding fraction ρ_t in the closure relation, which is the proportion of the surface area that is ponded and thus actively infiltrating. The potential infiltration depth over the ponded area of the REW, $I_{pp,t}$ (m), is defined as:

$$I_{pp,t} = \rho_t \cdot I_{p,t} \tag{12}$$

where $I_{p,t}$ (m) is the potential infiltration depth as calculated by the Green & Ampt model. The ponding fraction ρ_t is conceptualized as:

$$\rho_t = a \cdot S_{t-1} \tag{13}$$

with a (m^{-1}), an empirical scaling parameter, called a ponding factor. This parameter is used to represent the partial ponding areas within REWs after the rainstorm. During a rainstorm, the whole area of the REW is ponded (i.e. $\rho_t = 1$) due to the assumption of uniform infiltration parameters in the high resolution model. Therefore, Eq. (13) is only used for the period after the rainstorm

Table 2
Values of the inputs used to define the scenarios for the physically-based high resolution model.

Inputs	Description	Values			
		1	2	3	4
R_t	Rainfall intensity (m/h)	0.02	0.033	0.054	0.09
T	Duration of an event (h)	0.12	0.24	0.48	0.96
L	Slope length (m)	100.0	200.0	400.0	800.0
S_{avg}	Slope gradient (−)	0.02	0.06	0.18	0.54
K_s	Saturated hydraulic conductivity (m/h)	10^{-6}	0.005	0.013	0.035
θ_i	Initial moisture content (−)	0.05	0.1	0.2	0.4
H_f	Matric suction the wetting front (m)	−0.005	−0.012	−0.028	−0.066
c_1	Sill of the semivariogram model (m)	10^{-5}	2×10^{-4}	0.004	0.08

Table 3
Values of model inputs for all scenario runs in the high resolution model.

Inputs	Description	Values	Remarks
RR	Random roughness[a] (m)	0.004	Selected value for agricultural area with no tillage operation [53,54]
η	Effective porosity (−)	0.42	Typical value for silty clay soil [37]
n	Manning's roughness coefficient (h/m$^{1/3}$)	0.13	Typical value for a natural range land [44]
c_0	Nugget effect (m)	4.83×10^{-5}	Field observations
a	Range (m)	2.71	Field observations

[a] used for modeling depression storage by Eq. (3).

ceases. The actual infiltration depth $I_{a,t}$ (m) between $t-1$ and t is determined as the lesser value of the potential infiltration depth at t and the thickness of the water layer on the surface:

$$I_{a,t} = \min(I_{pp,t}, S_{f,t}) \tag{14}$$

where $S_{f,t}$ (m) is the depth of water on the surface available for infiltration at t, computed as:

$$S_{f,t} = R_{net,t} + S_{t-1} \tag{15}$$

Hortonian overland flow is modeled with a linear reservoir; i.e. discharge is a linear function of the amount of water on the surface, S_t. As runoff has to travel downhill, the hydrological responses (i.e. discharge) of the REW are, however, not instantaneous. Therefore, the travel time of runoff to the outlets is taken into account. This is done by using the past state of REW storage at a particular time preceding the current time to predict the discharge Q_t (m^3) at the time of interest:

$$\begin{aligned} Q_t &= (b \cdot S_{t-c}) \cdot A_{unit} \cdot \Delta t; \quad t > c \\ &= 0; \qquad\qquad\qquad\quad t < c \end{aligned} \tag{16}$$

where b (t^{-1}) is a reservoir parameter, c is a lag time index, S_{t-c} (m) is the depth of water layer on the surface at $t-c$, A_{unit} (m^2) is area of the REW. The lag time, c, represents the delay of the storage in releasing the water. If $t-c$ falls between two time steps, the value of S_t to be used is calculated by linear interpolation in time between S_t at the time step preceding $t-c$ and S_t at the succeeding $t-c$.

3.3. Calibration of the closure relation using the artificial data set

Step three in Fig. 1 is to calibrate the closure relation against the artificial data set produced by the high resolution model. This is done for each scenario run of the high resolution model, resulting in a set of scaling parameters for each scenario. The scaling parameters in the closure relation that are subject to calibration are the ponding factor (a) in Eq. (13), reservoir parameter (b) and lag time (c) in Eq. (16). Calibration of these parameters is done by minimizing the difference between the artificial data set and the results produced by the closure relation. The closure relation is calibrated using the data in each time step of 1 min.

Calibration of the ponding factor (a) is done by fitting a in Eq. (13) against average actual infiltration flux over the REWs in the artificial data set. We use a combination of a golden section search and successive parabolic interpolation for a continuous function for the calibration [55]. The calibration of a is only necessary for the period after the rainfall events because, during the events, the ponding factor is assumed constant (i.e. 1).

The calibration of parameter b and c is done with the shuffle complex evolution algorithm (SCE-UA). The SCE-UA method is a global optimization strategy which combines the simplex procedure with the concepts of controlled random search, competitive evolution and complex shuffling [56]. The reservoir parameter b and lag time c in Eq. (16) are fitted against the discharge in the artificial data set.

3.4. Deriving parameters in the closure relation directly from unit properties and rainstorm characteristics

Obviously, it is not practical to generate artificial data set to parameterize the closure relation for all REW units and rainstorms. Therefore, in the fourth step (Fig. 1), it is necessary to find a methodology to directly estimate the scaling parameters from the rainstorm characteristics and observable unit properties. As relations between physical properties of the REWs and the scaling parameters in the closure relations might theoretically exist [34], a set of scaling parameters for a given REW and rainstorm can be derived as a function of morphology and physical properties of REW. We explore two approaches in estimation of scaling parameters in the closure relation; a global method and local method (see Sections 3.4.1 and 3.4.2 below).

To validate the scaling parameter estimation approaches, the closure relation is tested with a set of 256 scenarios which have not been used in the calibration of the closure relation (i.e. independent scenarios). The independent scenarios are created using all possible combinations of physically-based high-resolution model inputs given in Table 4. Note that these values are different but within a range of those used in the calibration (Table 2).

3.4.1. Global method

In the global method, the scaling parameters: a, b and c, obtained by calibration are regressed against the REW and rainstorm characteristics used to create the scenarios in the high resolution

Table 4
Values of REW properties and rainfall characteristics used to define the scenarios for testing the closure relation.

Inputs	Description	Values	
R_t	Rainfall intensity (m/h)	0.049	0.072
T	Duration of an event (h)	0.18	0.45
L	Slope length (m)	375.0	600.0
S_{avg}	Slope gradient (−)	0.04	0.2
K_s	Saturated hydraulic conductivity (m/h)	0.0133	0.024
θ_i	Initial moisture content (−)	0.075	0.188
H_f	Matric suction the wetting front (m)	−0.008	−0.028
c_1	Sill of the semivariogram model (m)	1.05×10^{-4}	0.021

model (i.e. Table 1). The best multiple regression model is selected based on Mallow's C_p statistic [57]:

$$C_p = \frac{RSS_p}{\hat{\sigma}^2} + 2p + N, \tag{17}$$

where RSS_p is error sum of squares for the regression model with p predictors, where p is the number of predictors (i.e. model inputs), and N is sample size. The regression model with the smallest number of predictions is selected from those regression models with a C_p value equal to or smaller than the number of predictors in the regression model [57].

3.4.2. Local method

The local method only uses the information (i.e. parameter values) at the nearest locations in the parameter space to provide the predictions of parameters at the point of interest. We use the inverse distance method of interpolation to calculate the parameters at the unknown locations (i.e. a set of test scenarios in Table 4). The parameters at the unknown locations are interpolated based on the distance-weighted average of known data points in the neighborhood extent. The interpolation consists of 4 steps. First, the model inputs are standardized to equalize the range of model parameters in the parameter space. The second step is to select a set of neighbors (i.e. calibrated parameter values corresponding to the scenario runs in the high resolution model) for the given set of inputs from the test scenarios. This is done by selecting the scenario runs from the high resolution model whose model input values are at the adjacent upper or lower of the inputs values of the test scenarios. As the model has 8 independent inputs (Table 4), this results in $2^8 = 256$ neighbors to be used in the interpolation. The third step is to calculate the weight for each neighboring point, which is

$$w_i = d(x_0, x_i)^{-r} \tag{18}$$

where w_i is the weight assigned to a parameter value at the location x_i in the parameter space, $d(x_0,x_i)$ is the Euclidean distance in parameter space between the prediction location x_0 and the location x_i, r is a parameter. In the final step, the parameters at the unknown points can be interpolated as a weighted sum of the parameter values of N known points within the selected neighborhood:

$$\hat{\mathbf{U}}(x_0) = \frac{\sum_{i=1}^{N} w_i \cdot \mathbf{U}(x_i)}{\sum_{i=1}^{N} w_i} \tag{19}$$

where $\hat{\mathbf{U}}(x_0)$ represents the vector of interpolated values of the scaling parameters in the closure relation (i.e. a, b, c) at location x_0 (i.e. prediction location), $\mathbf{U}(x_i)$ is the vector of the calibrated scaling parameters in the closure relation at the location x_i, N is the number of neighboring points. If the interpolation points coincide with the data points, the parameters values at the data points are taken.

3.5. Evaluation criteria

As our interest is mainly on the hydrograph prediction in the REWs, evaluation of the closure relation is focused on the discharge (i.e. Hortonain runoff or concentrated overland flow). This also implies a good prediction in the total infiltration. The performance of the closure relation is evaluated in terms of the shape of the hydrograph, total discharge and peak discharge. For the shape of the hydrograph, the efficiency criterion proposed by Nash and Sutcliffe [58] is used:

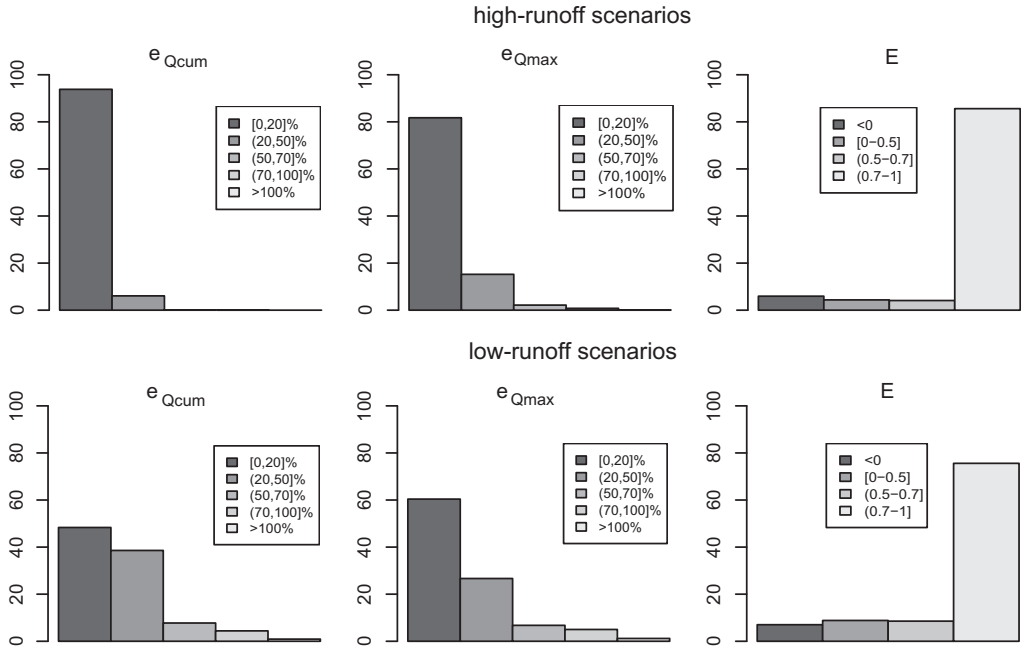

Fig. 4. Evaluation criteria of the closure relation using the calibrated scaling parameters. Top: high-runoff scenarios. Bottom: low-runoff scenarios. The length of the bars represents the percentage of scenarios that fall into the intervals of evaluation criteria, represented by individual bars.

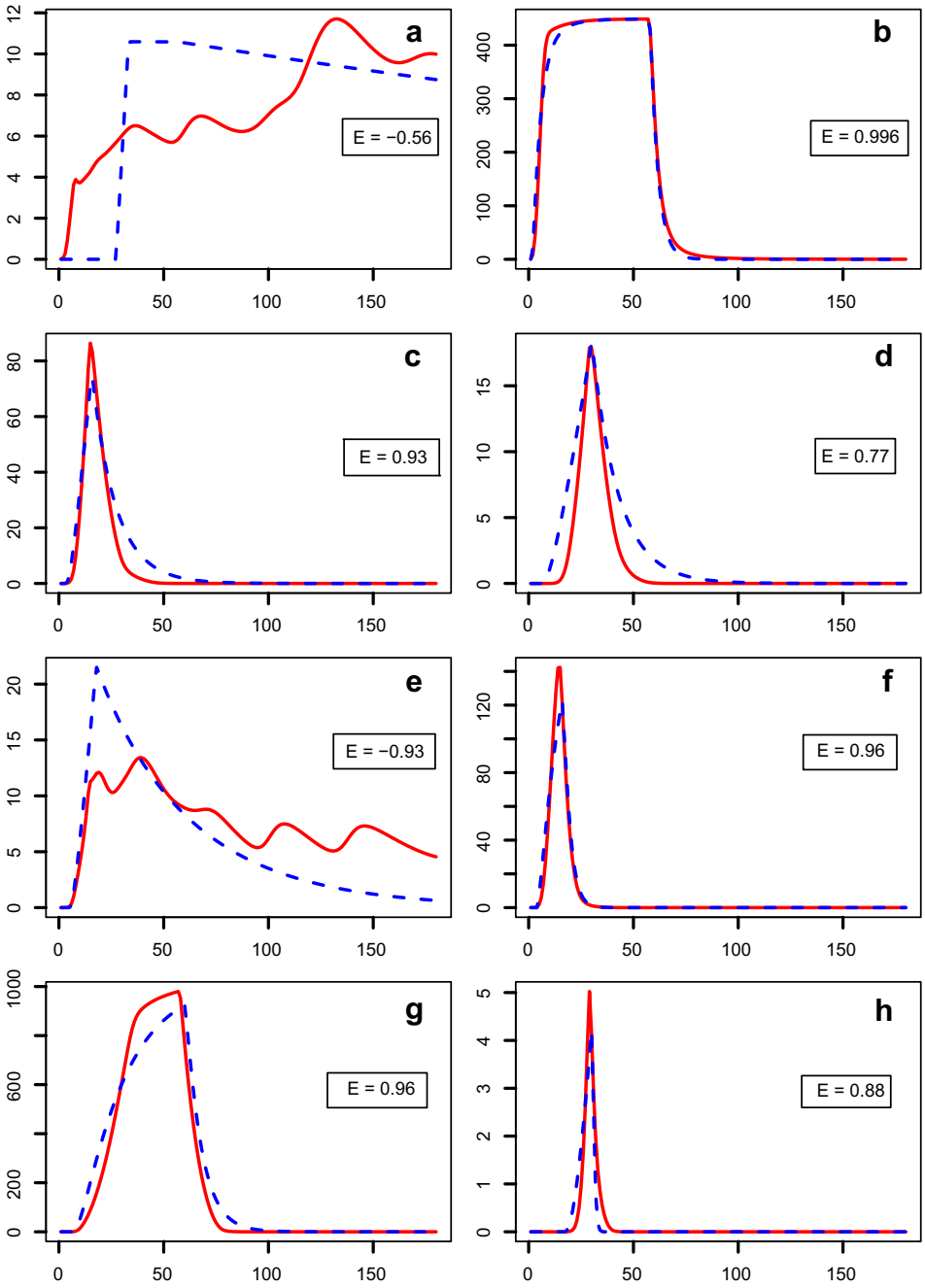

Fig. 5. Examples of hydrographs (y-axis: Q, m^3/h; x-axis: time, min) from the high resolution model (bold line) compared to hydrographs from the closure relation (dashed line) for the same set of model scenarios. The performance of the closure relation is evaluated by the Nash–Sutcliffe efficiency index (E).

Table 5
Details of scenario runs and evaluation assessment of the performance of the closure relation for the plots in Fig. 5.

Plots	Model inputs[a]								Evaluation assessment of the closure relation performance[b]		
	R_t	T	L	S_{avg}	K_s	H_f	θ_i	c_1	E	e_{Qcum}	e_{Qmax}
a	0.033	0.12	800	0.02	10^{-6}	−0.005	0.05	0.08	−0.56	8.93	9.49
b	0.09	0.96	100	0.54	10^{-6}	−0.028	0.05	10^{-5}	0.996	2.15	0.03
c	0.054	0.24	400	0.18	0.013	−0.012	0.1	2×10^{-4}	0.93	27.73	14.19
d	0.033	0.48	400	0.02	0.013	−0.012	0.2	10^{-5}	0.77	69.38	1.11
e	0.054	0.24	800	0.02	0.013	−0.012	0.2	0.004	−0.93	21.24	60.1
f	0.054	0.24	100	0.54	0.013	−0.012	0.2	10^{-5}	0.96	0.34	16.14
g	0.09	0.96	400	0.18	0.035	−0.028	0.2	2×10^{-4}	0.96	4.88	5.8
h	0.054	0.48	400	0.18	0.035	−0.028	0.2	2×10^{-4}	0.88	8.72	16.02

[a] For explanations of the symbols, see Table 2.
[b] E (−) is the Nash–Sutcliffe efficiency index. e_{Qcum} (%) and e_{Qmax} (%) is the percentage of absolute prediction error of total discharge and peak discharge, respectively.

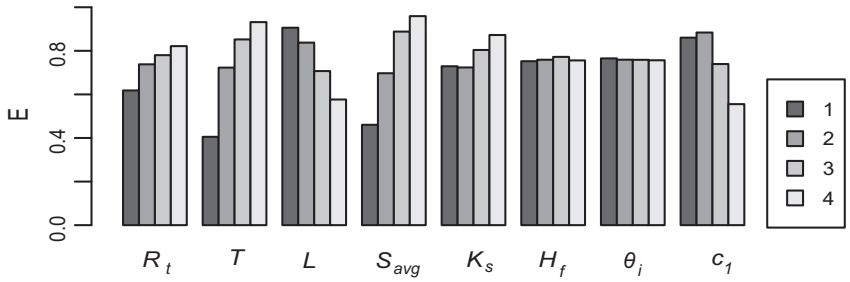

Fig. 6. Comparison of mean of E according to each value of inputs used to define the scenario runs. The numbers 1, 2, 3, 4 are the ordinal representation of the values in the series of each input, corresponding to the values in Table 2 (e.g. for R_t, '1' = 0.02 m/h, '2' = 0.033 m/h, '3' = 0.054 m/h, and '4' = 0.09 m/h and so on).

$$E = 1 - \frac{\sum_{t=1}^{T_{end}} (Q_{t,HR} - Q_{i,CR})^2}{\sum_{t=1}^{T_{end}} (Q_{t,HR} - \bar{Q}_{HR})^2} \quad (20)$$

where E (−) is Nash–Sutcliffe efficiency index, t is a simulation time steps, T_{end} is the end time of simulation (i.e. 3 h), $Q_{i,CR}$ (m^3/h) is the volume of discharge over a time unit calculated from the closure relation, $Q_{i,HR}$ (m^3/h) is the volume of discharge over a time unit calculated from the high resolution model, and $\bar{Q}_{HR}$ (m^3/h) is the mean discharge over the simulation time calculated from the high resolution model. The range of E values is between 1 and $-\infty$. A Nash–Sutcliffe efficiency index close to 1 indicates a good fit between the closure relation and the high resolution model. An efficiency index below zero implies that the mean value of the outputs of the high resolution model would have been a better predictor than the closure relation [59].

For the total discharge and peak discharge, the percentage of absolute prediction error between the outputs of the high resolution model and the results of the closure relation is used:

$$e_{Qcum} = \left| \frac{Q_{cum,HR} - Q_{cum,CR}}{Q_{cum,HR}} \right| \cdot 100 \quad (21)$$

$$e_{Qmax} = \left| \frac{Q_{max,HR} - Q_{max,CR}}{Q_{max,HR}} \right| \cdot 100 \quad (22)$$

where e_{Qcum} and e_{Qmax} (%) is the percentage of absolute prediction error of total discharge and peak discharge, respectively, $Q_{cum,HR}$ and $Q_{cum,CR}$ (m^3) is the total discharge of the high resolution model and closure relation, respectively, $Q_{max,HR}$ and $Q_{max,CR}$ (m^3/h) is the peak discharge of the high resolution model and closure relation, respectively.

4. Results

The results are presented for two groups of scenarios. The first group consists of the scenarios for which the percentage of runoff generated is between 0.5% and 10% of the net rain, referred to as 'low-runoff scenarios'. The second group contains the scenarios for which runoff generated is more than 10% of net rain: hereinafter 'high-runoff scenarios'. We do not consider scenarios with a runoff below 0.5% of net rain because our focus is on the events producing a significant amount of runoff.

Table 7
Regression coefficients and predictors[a] in the regression models for estimation of the scaling parameters.

Predictors	log(a)	log((b/0.5) + 0.05)	log(c + 0.005)
	Coefficient		
Intercept	4.038	3.678	−6.143
log(R_t)	−0.994	0.652	−0.3
log(T)	−0.564	0.468	0.007
log(L)	−0.4	−0.648	0.394
log(S_{avg})	0.248	0.428	−0.347
log(K_s)	0.029	−0.056	−0.03
log(abs(H_f))	0.037	−0.04	−0.008
log(θ_i)	−0.048	0.051	0.007
log(c_1)	−0.055	−0.016	0.069
r^2 [b]	0.723	0.758	0.578

[a] For explanations of the symbols, see Table 2. log() is the logarithmic transformation with natural base, abs() is absolute value.
[b] Adjusted r-squared values with a number of predictors in the models.

4.1. Direct calibration of the closure relation

For each scenario in the artificial data set, the outputs of the closure relation are compared with the outputs of the high resolution model to assess the ability of the closure relation in reproducing the high resolution model outputs.

In the evaluation of closure relation performance, 31% out of total scenarios (i.e. 65,536 scenarios) are disregarded because these scenarios produce a runoff less than 0.5% of net rain. As shown in Fig. 4, performance of the closure relation is satisfactory with regard to the shape of hydrograph, total volume of discharge and peak discharge for both high-runoff and low-runoff scenarios. It is clear that for the scenarios with a large amount of runoff, the closure relation performs better compared to the scenarios that produce a small amount of runoff. For more than 80% of the scenario runs in the high-runoff group, the prediction errors are less than 20% for total volume of discharge and peak discharge, and the Nash–Sutcliffe efficiency index falls between 0.7 and 1. The percentage of scenarios in the low-runoff group with good predictions (i.e. E index between 0.7 and 1 and prediction errors less than 20%) is smaller, particularly for the error in total discharge amount. The percentage of scenarios with less than 20% prediction error largely

Table 6
Descriptive statistics of the scaling parameters in the closure relation.

Parameters	Definition	Min	Mean	Max	Median	σ[a]	$C.V.$[b]	Skewness
a	Ponding factor	2.864	194.48	4980	132.63	209.16	1.075	4.05
b	Reservoir parameter	3.9×10^{-4}	0.05	0.303	0.03	0.047	0.94	1.6
c	Lag time	1.87×10^{-7}	0.11	0.65	0.067	0.119	1.08	2.22

[a] σ is standard deviation.
[b] $C.V.$ is coefficient of variation.

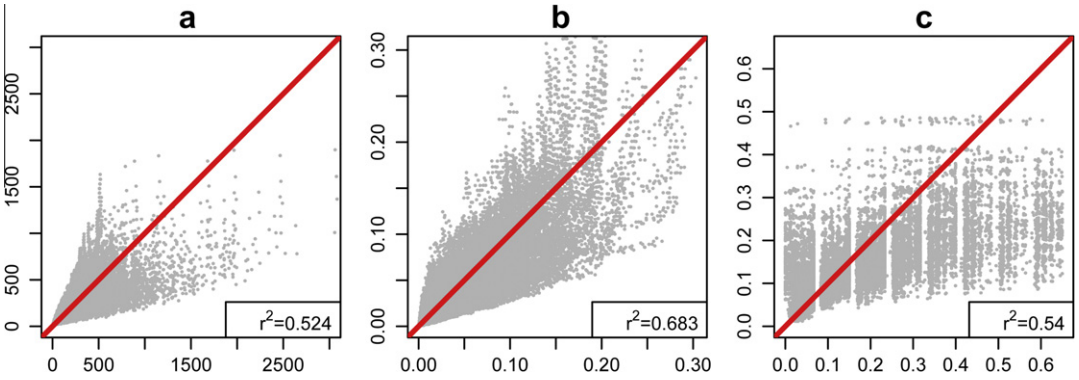

Fig. 7. 1:1 Plots of closure relation scaling parameters obtained by regression models (y-axis) versus those obtained by calibration (x-axis), including r^2 values. The red diagonal lines are 1:1 lines. (For interpretation of the references to colour in this figure legend, the reader is referred to the web version of this article.)

reduces from more than 90% for the high-runoff to 50% for the low-runoff group.

To illustrate the results, eight representative examples of hydrographs produced by the high resolution model compared to those simulated by the closure relation are shown in Fig. 5, including the details of scenario runs of each comparison plot and the evaluation assessment of closure relation performance (Table 5). In general, the closure relation is capable of reproducing the hydrographs in the artificial data set. A preliminary conclusion can be drawn. The performance of the closure relation increases with (1) an increase in the amount of runoff produced and (2) a decrease in variance of the hydrologic responses (i.e. degree of instantaneousness of responses).

Regarding the amount of runoff generated, the events with a high amount of discharge generated (e.g. Fig. 5(b), (f) and (g)) have an efficiency index E close to 1. This indicates an almost perfect fit between the closure relation and the high resolution model. The closure relation performance tends to decrease when generated runoff is small (e.g. Fig. 5(a) and (e)). Fig. 5(c) and (d) exemplify the effect of increasing the timing of hydrologic responses on increasing in the closure relation performance. The hydrograph is better predicted for the case of fast discharge responses (Fig. 5(c)) compared to the case of slow discharge responses (Fig. 5(d)). For the geometry of REWs, with similar rainstorm and infiltration characteristics, discharge is better simulated for a unit with a geometry resulting in more instantaneous response (Fig. 5(f)), compared to a unit whose geometry decelerates the runoff response (Fig. 5(e)). For the rainstorm characteristics, the closure relation gives better results for a larger event (Fig. 5(g)) compared to a smaller event (Fig. 5(h)), regardless of the unit geometry and infiltration properties of REWs. This is because increasing the amount of rainfall leads to an increase of runoff generated as well as flow velocity of runoff; and consequently, fast timing of responses. The joint effects of rainstorm characteristics

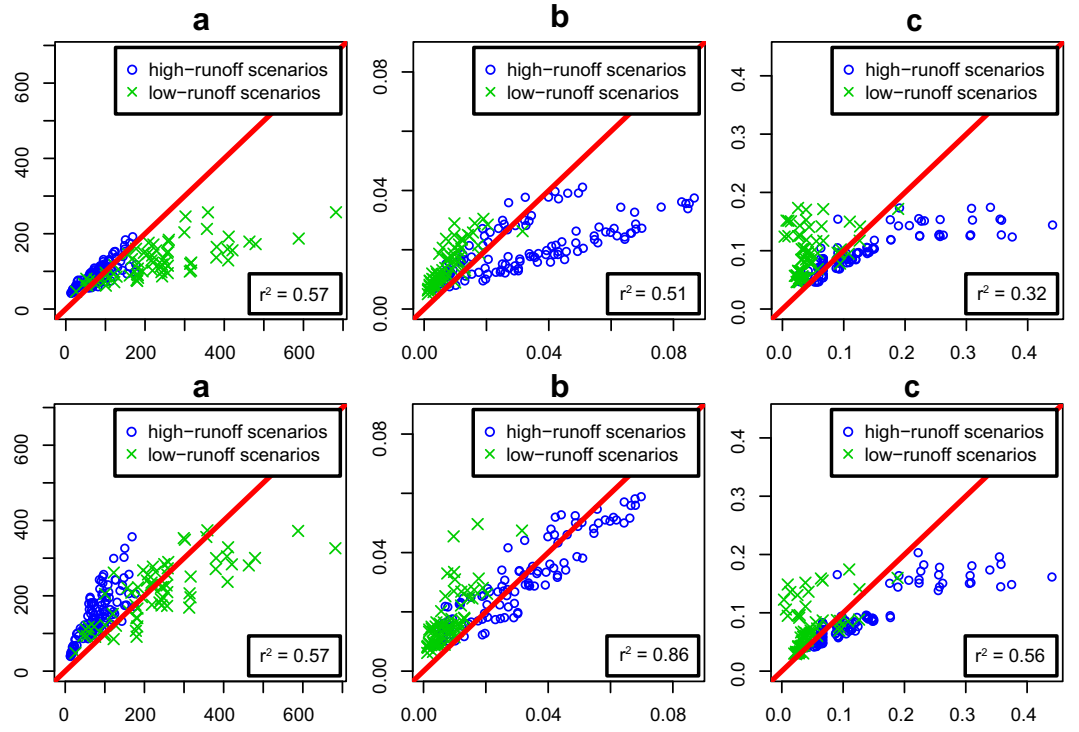

Fig. 8. Scaling parameters in the closure relation obtained by the regression models (y-axis, top) and by inverse distance weighted interpolation method (y-axis, bottom) versus calibrated parameters (x-axis) for the test scenarios. The plots in the first, second, and third column are the comparison plots of parameter a, b, c, respectively.

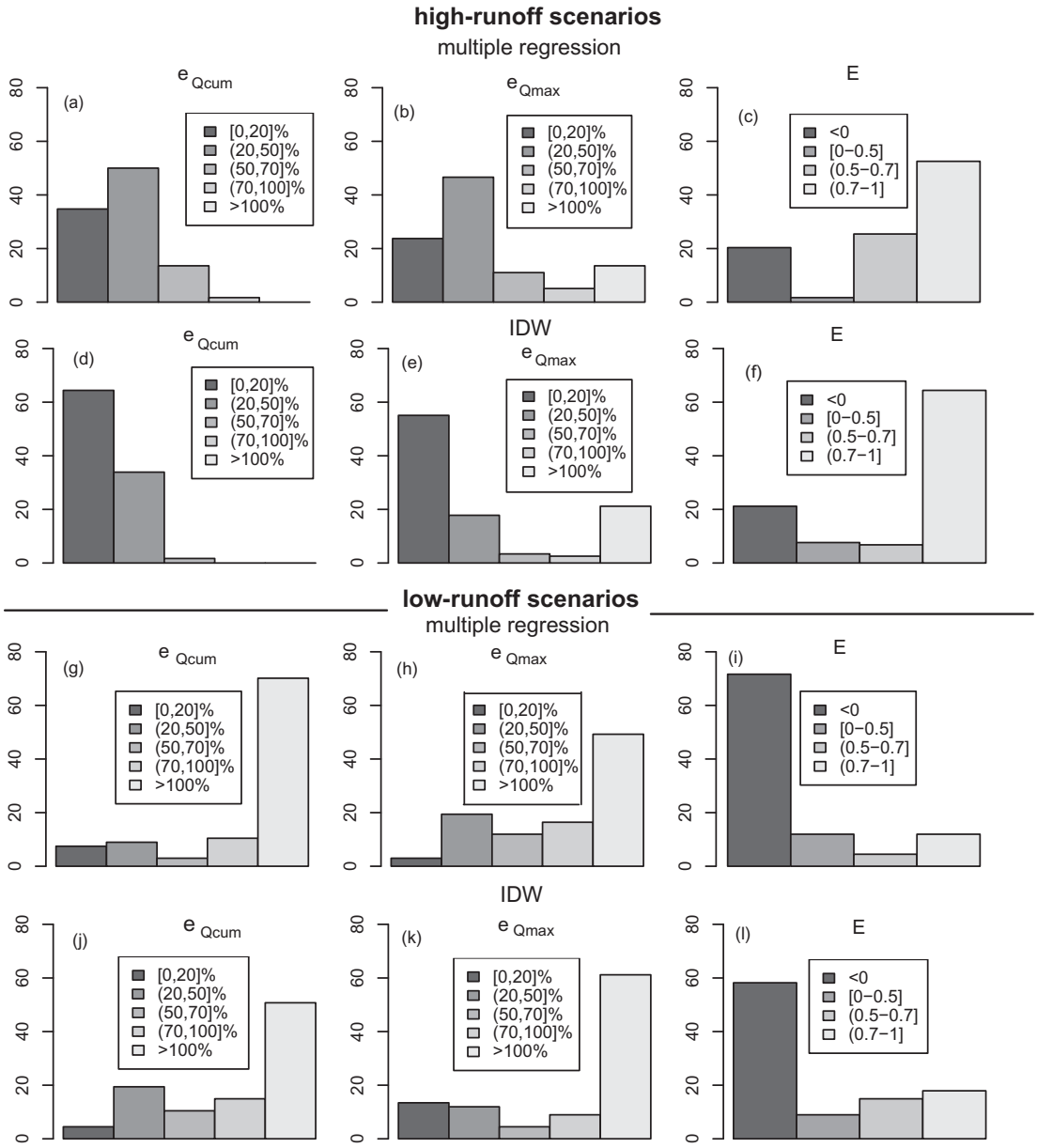

Fig. 9. Evaluation criteria of the closure relation using the scaling parameters derived from the regression method (plots in row 1 and 3: a–c and g–i) and from the inverse distance weighted interpolation method (IDW; plots in row 2 and 4: d–f and j–l). The length of the bars represents the percentage of scenarios that fall into the intervals of evaluation criteria, represented by individual bars.

and unit geometry to the closure relation performance result in either maximizing (Fig. 5(b)) or minimizing (Fig. 5(a)) the closure relation performance.

To gain more insight into the nature of closure relation performance, mean values of E, e_{Qcum} and e_{Qmax} are calculated for each value of the independent model variables (i.e. the inputs of high resolution model). Because the results are similar for all evaluation criteria, Fig. 6 shows E values only. The performance of the closure relation increases with increasing rainfall intensity, event duration, slope gradient; and decreasing slope length and variation of micro relief; that is, units with an almost parallel flow pattern (Fig. 3, left). From this analysis, it can be concluded that the performance of the closure relation is mainly determined by the fastness of hydrologic responses and yields best prediction results when hydrological responses are almost instantaneous (Fig. 5(a), (f) and (h)). Although not shown, we can also conclude that the prediction error of peak discharge is, in general, slightly larger than the prediction error of the total amount of discharge.

4.2. Arbitrarily-defined REWs and rainstorms: using the estimated scaling parameters

Here, the closure relation performance is evaluated for the set of arbitrarily-defined REWs or independent runs where scaling parameters in the closure relation have been estimated from observable REW properties and rainstorm characteristics (Table 4), 28% of the total test scenarios are excluded from the analysis due to the insignificant amount of runoff produced (i.e. runoff less than 0.5% of net rain). As before, the closure relation is evaluated by comparing its outputs against the results from the high resolution model.

4.2.1. Testing the approaches for estimations of scaling parameters

4.2.1.1. Global method.

The descriptive statistics of scaling parameters from calibrating the closure relation to outputs of the high-resolution model (i.e. exclusive the scenarios with a runoff less than 0.5% of net rain to avoid

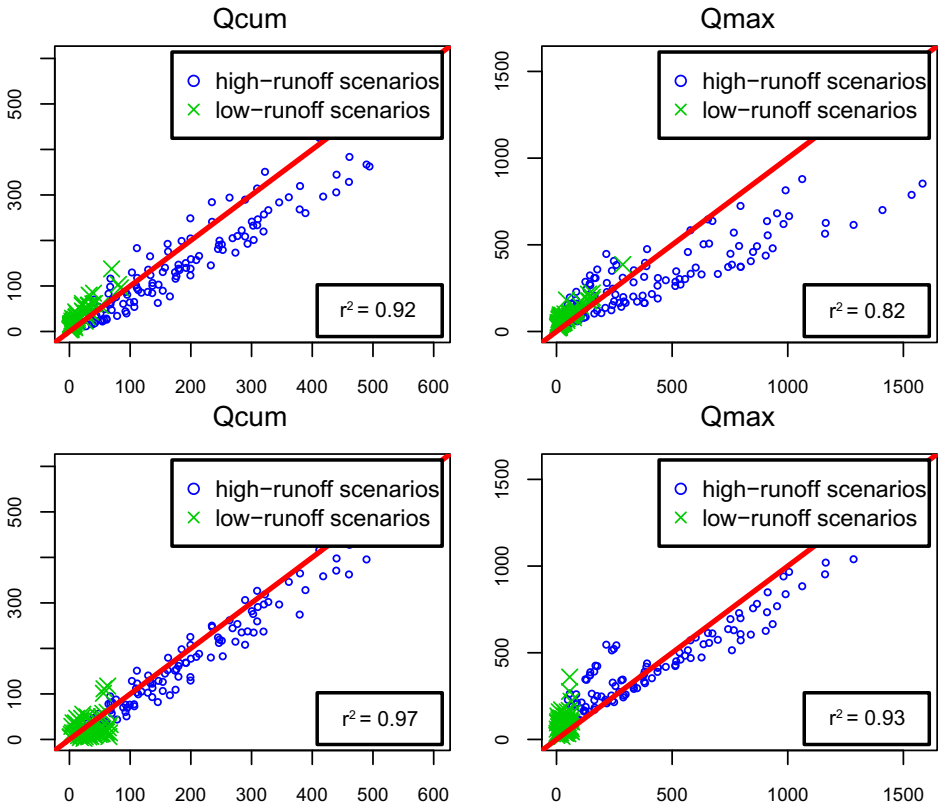

Fig. 10. Total discharge volume (Q_{cum}, left) and peak discharge (Q_{max}, right) obtained by the closure relation with parameters estimated by multiple regression (y-axis, top) and by inverse distance weighted interpolation (y-axis, bottom) versus the results of the high-resolution model (x-axis).

the effects of outliers and extremely high parameter values in the regression models) (Table 6) depict a relatively large range of parameter values. The distributions of all scaling parameters in the closure relation are positively skewed. The chi-square test rejects the null hypothesis of a normal distribution at a 95% confidential level for all scaling parameters. Hence, the values of scaling parameters must be transformed (i.e. logarithmically or algebraically) such that the parameters are approximately normally distributed. The values of independent variables (i.e. model inputs) are subject to the transformation as well because the distribution of original values of independent variables can be highly skewed for two reasons. First, the model inputs are defined as geometric series. Second, the exclusion of parameters of no-runoff scenarios has an effect on the distribution of model inputs. The regression models for each scaling parameter including the r^2 values are shown in Table 7. Model inputs are all log-transformed while transformation of dependent variables (i.e. scaling parameters in the closure relation) is chosen based on trial and error such that a normal distribution is obtained.

According to the Mallow's C_p statistics, all independent variables (i.e. model inputs used to create scenario runs in the high resolution model) should be used as predictors in the regression models. The adjusted r-square values shows that the variances explained by the regression models are larger for transformed ponding factor a and reservoir parameters b compared to the transformed values of lag time c.

For ponding factor (a), it is difficult to explain the direction of the relation between the independent variables and the ponding factor a (i.e. negative or positive, Table 6) through the regression coefficients. The ponding factor is defined as a product of ponding factor and surface water (Eq. (13)), so a determines the slope of the ponding fraction curve. The value of a increases with the degree of change in ponding fraction or, say, the discharge generation rate. Discharge response is more instantaneous when the units have parallel flow pattern, associated with a steep slope gradient and small variation of micro relief. Therefore, a has a positive relation with slope gradient and negative relation with variation in micro relief.

The reservoir parameter (b) is large when a large amount of runoff is generated. Therefore, the reservoir parameter has a positive relation with rainfall intensity, event duration, slope gradient, and antecedent moisture content. A negative relation is found with slope length, saturated hydraulic conductivity, positive values of matric suction at the wetting front and variation in micro relief.

For the lag time (c), it is expected that the regression coefficients are negative for the event duration and antecedent moisture content; while positive for saturated hydraulic conductivity and matric suction at the wetting front. This is because the hydrologic responses are more instantaneous (i.e. lag time is small) when event duration is long (i.e. more water to the system) and infiltration capacity is small (i.e. decrease in saturated hydraulic conductivity and decrease in matric suction at the wetting front. However, the regression coefficients are the opposite (i.e. positive for event duration and negative for saturated hydraulic conductivity and matric suction at the wetting front).

The parameter values obtained from the regression models are back transformed and plotted against the corresponding calibrated values (Fig. 7). With the non-transformed parameters, the plots show a slight decrease in the agreement between the calibrated parameter values and the values predicted by the regression models. Only 50% of variance is explained by the regression models for a and c; while 68.3% of variance of b is explained.

4.2.1.2. Local method. The inverse distance weighted method was tested with different power r values (Eq. (18)), and we found that the best results were obtained with r equal to 3. It should be noted that there are abrupt changes of parameter values at the locations

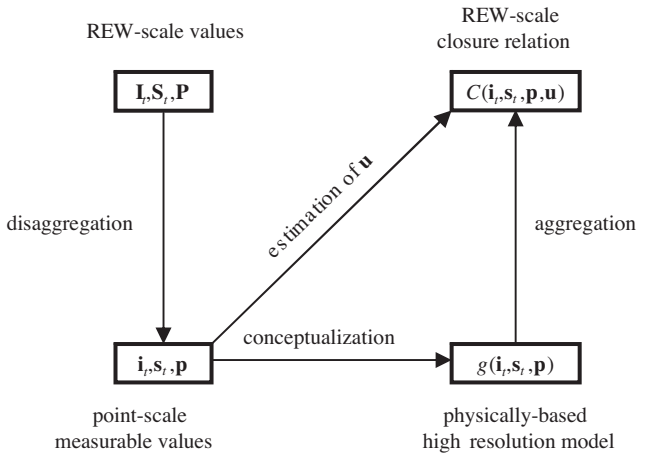

Fig. 11. Schematic figure of the development of the closure relation for Hortonian runoff in the context of the disaggregation–aggregation framework proposed by Viney and Sivapalan [61]. The uppercase symbols denote the variables or functions at the REW scale while the lowercase symbols are for the local (point) scale. $\mathbf{I}_t$, $\mathbf{i}_t$ are the input; $\mathbf{S}_t$, $\mathbf{s}_t$ are state variables; $\mathbf{P}$, $\mathbf{p}$ are parameters. g and C are process conceptualizations (i.e. physically-based high resolution model and closure relation, respectively). $\mathbf{u}$ is a set of scaling parameters.

close to the edges (i.e. either left or right) of the parameter space. These parameter values are considered as outliers because they belong to the scenarios with insignificant amount of runoff generated (i.e. runoff less than 0.5% of net rain). It turned out to be necessary to remove these parameter values to avoid the influences of these extreme parameter values in the interpolation if the point of interpolation is close to the edges of the parameter space. Therefore, most of the test scenarios (i.e. Table 4) have relatively small neighborhood size, ranging from 21 to 232 points.

4.2.2. Estimation of the closure relation parameters

Fig. 8 shows that compared to the multiple regression method, the inverse distance interpolation method gives better results in estimating scaling parameters of the test scenarios data set. For parameter *a*, both approaches give equally good predictions. However, the inverse distance weighted interpolation method largely improves the predictions of parameter *b* and *c*. For the low-runoff scenarios group, *a* is underestimated while *b* and *c* are overestimated. The parameter predictions for the high-runoff scenarios group show the opposite results. Predictions of *c* is underestimated while *a* is overestimated only using the inverse distance weighted interpolation method.

4.2.3. Hydrograph prediction

When considering reproduction of hydrographs, as expected, the closure relation using the estimated scaling parameters shows a lower performance than the closure relation with the calibrated scaling parameters, as manifested by the decrease in the percentage of scenarios with a good fit between the closure relation and high resolution model (Figs. 4 and 9). In general, the closure relation performance using the estimated scaling parameters is larger for the high-runoff group than for the low-runoff group, regardless of the methods of parameter estimation. This finding is similar to the closure relation using the calibrated scaling parameters (i.e. Section 4.1). Fig. 9 also shows that the closure relation with parameters estimated by inverse distance weighted interpolation has superior performance to the closure relation that uses the regression models to estimate its parameters. For both low-runoff and high-runoff scenarios groups, the percentages of scenarios that fall into a class of 'small' prediction errors (i.e. e_{Qcum} and e_{Qmax} below 20% and *E* index above 0.7) are lower for the case of the closure relation that uses parameters based on regression. However, errors in the peak discharge prediction in the low-runoff scenarios group are exceptions (Fig. 10(h) and (k)).

The comparison between the total discharge volume as well as the peak discharge calculated by the closure relation and those produced by the high-resolution model (Fig. 10) supports the findings that the closure relation performs better when its parameters have been obtained by the inverse distance weighted interpolation.

As with the results of the closure relation with calibrated scaling parameters, the prediction of total discharge volume is more accurate than the peak discharge.

5. Discussion and conclusion

In this study, we propose and evaluate a closure relation for infiltration-excess overland flow (i.e. infiltration and Hortonian runoff flux) in the REW context. The closure relation is developed as a lumped conceptual model that calculates the cross-boundary flux as a function of input flux, a current and past state of storage in the REWs, point-scale measurable physical properties, and a set of scaling parameters describing the effects of scale transfer (i.e. REW geometry and sub-REW scale heterogeneity in processes and measurable physical properties). These scaling parameters can be derived from observable REW physical characteristics, geometry, state variables as well as the boundary conditions. The past trajectory of the input flux is neglected in the derivation of the scaling parameters in this study.

The closure relation for infiltration and Hortonian runoff is derived following the numerical simulation approach. In doing so, an extensive set of cross-boundary flux (i.e. rainfall, infiltration, overland flow) and internal states for a large range of hypothetic REWs and rainstorms was generated by a physically-based high resolution model. This synthetic data set provides complete knowledge of all states and fluxes for a wide range of catchment and rainstorm characteristics that could not be obtained from measurements. Furthermore, with the use of a high resolution model, point-scale measurable values can be used throughout the procedure. The closure relation consists of the standard form of the Green & Ampt equation and a linear reservoir describing the infiltration and Hortonian runoff flux respectively. The closure relation uses three scaling parameters; a ponding factor, a reservoir parameter, and a lag time.

The results show that the closure relation *C* for infiltration and Hortonian runoff can be identified and parameterized using the synthetic data set. The closure relation is capable of reproducing the Hortonian runoff for an extensive range of scenarios of REWs and individual storms when calibrated for each scenario. More than 80% of the 'high-runoff' scenarios and about 75% of the 'low-runoff' scenarios have a Nash-Sutcliffe efficiency index between 0.7 and 1.0 (Fig. 4). The performance of the closure relation reduces when a small amount of runoff is generated and when the hydrologic responses are not instantaneous. This situation occurs with a small rainstorm, high infiltration capacity, and REWs with a geometry decelerating runoff responses (i.e. large slope length, high slope gradient, and a large variation in micro relief resulting in a random flow pattern). Under these conditions, spatial processes in runoff generation (i.e. interaction between infiltration, runon and runoff) become important. The closure relation does not explicitly consider such spatial interactions as it is fundamentally a lumped conceptual model, resulting in a lower performance for the group of 'low-runoff' scenarios.

Regarding the estimation of the scaling parameters from the observable REW properties and rainstorm characteristics, a local approach (see Fig. 8), using inverse distance weighted interpolation in the parameter space, outperforms the regression method. The local method gives better estimates of all scaling parameters in

the closure relation, except for the ponding factor a, resulting in a better discharge prediction compared to the regression method. In the independent runs, 65% of the events in the 'high-runoff' scenario has a Nash- Sutcliffe efficiency index between 0.7 and 1.0, with the scaling parameters estimated by the local method. This percentage decreases to 50% when the global method is used to estimate the scaling parameters. These findings indicate a considerable degree of non-linearity in the parameter space; the multiple linear regression technique is apparently not sufficient to describe the relations, especially at the edges of the parameter space where the scaling parameters for the 'low-runoff' scenarios are located. This non-linearity may be due to the spatial heterogeneity in the infiltration process in the Hortonain runoff generation mechanism that becomes more important in the 'low-runoff' scenarios and, hence, complicates the tasks of scaling parameter estimation by the regression method [34]. Here, we conclude that the relation between the scaling parameters and observational parameters is non-linear and can be best described using the local information in the parameter space.

It is expected that the discharge predictions would be more accurate if estimation errors of scaling parameters in the closure relation are further reduced. To reduce the errors, it is recommended to use more points in the parameter space, which means that a larger artificial data set is required. Focus should be more on scenarios producing a small amount of runoff because these scenarios are located near the edge of the parameter space, where the parameter values may exhibit a strong non-linear change. Another option would be to employ other data transformation techniques and use other parameter estimation methods.

The development of the closure relation in this study partly follows the disaggregation–aggregation approach originally proposed by Robinson and Sivapalan [60] and later schematically presented in Viney and Sivapalan [61]. Robinson and Sivapalan [60] proposed to estimate the REW scale closure relation from REW scale values. Here, we propose a different approach where REW scale closure relation are derived from local-scale measureable values. As we assume uniform meteorological forcing and unit properties, the disaggregation of REW-scale variables $\mathbf{I}_t$, $\mathbf{S}_t$, $\mathbf{P}$ to local-scale values $\mathbf{i}_t$, $\mathbf{s}_t$, $\mathbf{p}$ is neglected in our study. Using local-scale values, we use a physically-based high resolution model to represent the processes g at the local scale. For the process conceptualization at the REW scale (i.e. the closure relations C), we use for infiltration the same form of process conceptualization as used at the local scale, and for runoff we identify a new form of process conceptualization (i.e. a linear reservoir with lag time). This requires an additional set of parameters to compensate the scale transfer effects, called scaling parameters $\mathbf{u}$. Aggregation of the local-scale processes to REW scale processes is done by generating an extensive data set of hydrologic responses with the high-resolution model. The scaling parameters $\mathbf{u}$ in the closure relations C are found by calibration against this synthetic data set. Finally, a multiple regression and a local interpolation method are proposed that allow direct estimation of the REW-scale scaling parameters from local-scale values (diagonal line in Fig. 11). Note that this is different from the approach described by Viney and Sivapalan [61], as their approach proposes to estimate the scaling parameters of the closure relation from REW-scale values. Thus, our approach is feasible mainly when local scale values have been observed, or when appropriate disaggregation methods to downscale REW-scale values to local-scale values are available. The development of a closure relation following our approach can also be considered as identifying a dynamic emulation model that a reduced order emulation (i.e. closure relations) of the higher order simulation model (i.e. high resolution model) is developed based on the analysis of data obtained from planned experiments using the simulation model in the context of database mechanistic and top-down modeling [62].

The limitation of this study is mainly the limited physics used in the high resolution model. Due to the limited computational resources, it was not possible to represent the processes at the local scale using fully physically-based process descriptions (e.g. Darcy–Richard equations or multi-layer infiltration model), as this would considerably increase model run time. Also, spatio-temporal variability of parameters within the REWs was partly neglected, although runoff was considered spatially variable. Incorporating spatio-temporal variation in parameters of the high resolution model would introduce additional parameters describing the higher order statistics of the parameters. This would significantly increase the number of runs required with the high-resolution model, as a much larger parameter space would need to be filled. However, both using more physics and incorporating spatial variation are possible within our proposed framework. The only requirement would be large computational resources (cluster computations).

It might be needed to incorporate more key processes related to Hortonian runoff generation mechanism in the closure relation. For example, several studies have shown that the surface storage may influence the Hortonian runoff generation in agricultural areas (e.g. [39]). Thus, parameters related to surface roughness such as Manning's roughness coefficient, soil porosity and surface roughness index should be considered in creating the artificial data set in the high resolution model. Surface storage processes should, hence, be explicitly considered in the closure relation as well as in the estimation of scaling parameters. Furthermore, this study does not consider other discharge generation processes, such as the saturated overland flow and subsurface flow, which play an important role in the runoff generation in the low-lying slopes and humid catchments.

Finally, it is important to assess the value and applicability of the closure relation in real-world cases. This involves testing the closure relation against the field data (i.e. discharge). Inputs and boundary conditions required in the closure relations can be obtained from field observations (i.e. rainfall, REW properties) or estimated using a simple model (i.e. evapotranspiration model to estimate initial soil moisture content). The application and evaluation of our approach for real world data is now ongoing and will be reported in a subsequent paper.

References

[1] Beven K, Freer J. A dynamic TOPMODEL. Hydrol Process 2001;15(10):1993–2011.

[2] Reggiani P, Sivapalan M, Majid Hassanizadeh S. A unifying framework for watershed thermodynamics: balance equations for mass, momentum, energy and entropy, and the second law of thermodynamics. Adv Water Resour 1998;22(4):367–98.

[3] Reggiani P, Hassanizadeh SM, Sivapalan M, Gray WG. A unifying framework for watershed thermodynamics: constitutive relationships. Adv Water Resour 1999;23(1):15–39.

[4] Tian F, Hu H, Lei Z, Sivapalan M. Extension of the Representative Elementary Watershed approach for cold regions via explicit treatment of energy related processes. Hydrol Earth Syst Sci 2006;10(5):619–44.

[5] Li H, Sivapalan M. Effect of spatial heterogeneity of runoff generation mechanisms on the scaling behavior of event runoff responses in a natural river basin. Water Resour Res 2011;47(January):1–20.

[6] Lee H, Sivapalan M, Zehe E. Representative Elementary Watershed (REW) approach, a new blueprint for distributed hydrological modelling at the catchment scale. In: Franks SW, Sivapalan M, Takeuchi K, Tachikawa Y, editors. Predictions in Ungauged Basins: International Perspectives on the State of the Art and Pathways Forward, 301. Mepple: IAHS Publication; 2005. p. 159–88.

[7] Beven K. Searching for the Holy Grail of scientific hydrology: $Q_t = (S, R, \Delta t)A$ as closure. Hydrol Earth Syst Sci 2006;10(5):609–18.

[8] Lee H, Zehe E, Sivapalan M. Predictions of rainfall-runoff response and soil moisture dynamics in a microscale catchment using the CREW model. Hydrol Earth Syst Sci 2007;11(2):819–49.

[9] Reggiani P, Rientjes THM. Flux parameterization in the representative elementary watershed approach: application to a natural basin. Water Resour Res 2005;41(4):1–18.

[10] Zhang G, Savenije H. Rainfall-runoff modelling in a catchment with a complex groundwater flow system: application of the Representative Elementary Watershed (REW) approach. Hydrol Earth Syst Sci 2005;9(3):243–61.
[11] Zhang GP, Savenije HHG, Fenicia F, Pfister L. Modelling subsurface storm flow with the Representative Elementary Watershed (REW) approach: application to the Alzette River Basin. Hydrol Earth Syst Sci 2006;3(1):229–70.
[12] Zehe E, Lee H, Sivapalan M. Dynamical process upscaling for deriving catchment scale state variables and constitutive relations for meso-scale process models. Hydrol Earth Syst Sci 2006;10(6):981–96.
[13] Mou L, Tian F, Hu H, Sivapalan M. Extension of the Representative Elementary Watershed approach for cold regions: constitutive relationships and an application. Hydrol Earth Syst Sci 2008;12(2):565–85.
[14] Tian F, Hu H, Lei Z. Thermodynamic watershed hydrological model: constitutive relationship. Sci China Ser E Technol Sci 2008;51(9):1353–69.
[15] Karssenberg D. Upscaling of saturated conductivity for Hortonian runoff modelling. Adv Water Resour 2006;29(5):735–59.
[16] Troch PA. Hillslope-storage Boussinesq model for subsurface flow and variable source areas along complex hillslopes: 1. Formulation and characteristic response. Water Resour Res 2003;39(11):1316.
[17] Hilberts AGJ, van Loon EE, Troch PA, Paniconi C. The hillslope-storage Boussinesq model for non-constant bedrock slope. J Hydrol 2004;291(3–4):160–73.
[18] Bogaart PW, Troch PA. Curvature distribution within hillslopes and catchments and its effect on the hydrological response. Hydrol Earth Syst Sci 2006;10(6):925–36.
[19] Varado N, Braud I, Galle S, Le Lay M, Séguis L, Kamagate B, Depraetere C. Multi-criteria assessment of the Representative Elementary Watershed approach on the Donga catchment (Benin) using a downward approach of model complexity. Hydrol Earth Syst Sci 2006;10(3):427–42.
[20] Xu C. Testing the transferability of regression equations derived from small sub-catchments to a large area in central Sweden. Hydrol Earth Syst Sci 2003;7(3):317–24.
[21] Yokoo Y, Kazama S, Sawamoto M, Nishimura H. Regionalization of lumped water balance model parameters based on multiple regression. J Hydrol 2001;246(1–4):209–22.
[22] Duffy CJ. A two-state integral-balance model for soil moisture and groundwater dynamics in complex terrain. Water Resour Res 1996;32(8):2421.
[23] Corradini C, Morbidelli R, Melone F. On the interaction between infiltration and Hortonian runoff. J Hydrol 1998;204(1–4):52–67.
[24] Stomph TJ, de Ridder N, Steenhuis TS, Van de Giesen NC. Scale effects of Hortonian overland flow and rainfall-runoff dynamics: laboratory validation of a process-based model. Earth Surf Proc Land 2002;27(8):847–55.
[25] Wallach R, Grigorin G, Byk J. The errors in surface runoff prediction by neglecting the relationship between infiltration rate and overland flow depth. J Hydrol 1997;200(1–4):243–59.
[26] Silberstein R. Hydrological models are so good, do we still need data? Environ Model Softw 2006;21(9):1340–52.
[27] Wetzel PJ, Liang X, Irannejad P, Boone A, Noilhan J, Shao Y, Skelly C, Xue Y, Yang ZL. Modeling vadose zone liquid water fluxes: infiltration, runoff, drainage, interflow. Global Planet Change 1996;13(1–4):57–71.
[28] Vereecken H, Huisman JA, Bogena H, Vanderborght J, Vrugt JA, Hopmans JW. On the value of soil moisture measurements in vadose zone hydrology: a review. Water Resour Res 2008;44:1–21.
[29] Weiler M, Mcdonnell J. Virtual experiments: a new approach for improving process conceptualization in hillslope hydrology. J Hydrol 2004;285(1-4):3–18.
[30] Wood EF, Bool J, Bogaart P, Troch P. The need for a virtual hydrologic laboratory for PUB. In: Franks SW, Sivapalan M, Takeuchi K, Tachikawa Y, editors. Predictions in Ungauged Basins: International Perspectives on the State of the Art and Pathways Forward, 301. Mepple: IAHS Publication; 2005. p. 189–203.
[31] Bashford KE, Beven KJ, Young PC. Observational data and scale-dependent parameterizations: explorations using a virtual hydrological reality. Hydrol Process 2002;16(2):293–312.
[32] Loague K, Abrams RH. Stochastic-conceptual analysis of near-surface hydrological response. Hydrol Process 2001;15(14):2715–28.
[33] Mirus BB, Loague K, Cristea NC, Burges SJ, Kampf SK. A synthetic hydrologic-response dataset. Hydrol Process 2011;25(23):3688–92.
[34] Kling H, Gupta H. On the development of regionalization relationships for lumped watershed models: the impact of ignoring sub-basin scale variability. J Hydrol 2009;373(3–4):337–51.
[35] Abbott MB, Bathurst JC, Cunge JA, O'Connell PE, Rasmussen J. An introduction to the European Hydrological System – Systeme Hydrologique Europeen, "SHE", 1: History and philosophy of a physically-based, distributed modelling system. J Hydrol 1986;87(1-2):45–59.
[36] Karssenberg D, de Jong K, van der Kwast J. Modelling landscape dynamics with Python. Int J Geogr Inf Sci 2007;21(5):483–95.
[37] Rawls WJ, Brakensiek DL, Miller N. Green–Ampt infiltration parameters from soils data. J Hydraul Eng ASCE 1983;109(1):62.
[38] Saghafian B, Julien PY, Ogden FL. Similarity in catchment response: 1. Stationary rainstorms. Water Resour Res 1995;31(6):1533.
[39] Onstad CA. Depressional storage on tilled surfaces. Trans ASAE 1984;27(3):729–32.
[40] Govers G, Takken I, Helming K. Soil roughness and overland flow. Agronomie 2000;20(2):131–46.
[41] Allmaras RR, Burwell RE, Larson WE, Holt RF. Total porosity and random roughness of the interrow zone as influenced by tillage. In: USDA Conservation Res. Rep. 7, Washington, DC; 1966, p. 1–22.
[42] Meng H, Green T, Salas J, Ahuja L. Development and testing of a terrain-based hydrologic model for spatial Hortonian Infiltration and Runoff/On. Environ Model Softw 2008;23:794–812.
[43] Kazezyılmaz-Alhan CM, Medina MA. Kinematic and diffusion waves: analytical and numerical solutions to overland and channel flow. J Hydraul Eng ASCE 2007;133(2):217.
[44] Chow VT, Maidment DR, Mays LW. Applied hydrology. New York: McGraw Hill; 1988.
[45] Burrough PA, McDonnell RA. Principles of geographical information systems. 5th ed. New York: Oxford University Press; 2004.
[46] Merriam RA. A note on the interception loss equation. J Geophys Res 1960;65(11):3850.
[47] von Hoyningen-Huene J, Die Interzeption Des Niederschlags. In: Landwirtschaftlichen Pflanzenbeständen, DVWK: Brunswick, Arbeitsbericht DeutscherVerband fürWasserwirtschaft und Kulturbau; 1981.
[48] Kuriakose SL, van Beek LPH, van Westen CJ. Parameterizing a physically based shallow landslide model in a data poor region. Earth Surf Proc Land 2009;34(6):867–81.
[49] Bierkens MFP, Finke PA, de Willigen P. Upscaling and downscaling methods for environmental research. Dordrecht: Kluwer; 2000.
[50] Vannametee E. Upscaling of hydrological processes for an alluvial fan: fundamental knowledge for hydrogeomorphic-based catchment modelling. Utrecht University; 2008.
[51] Pebesma EJ, Heuvelink GBM. Latin hypercube sampling of Gaussian random fields. Technometrics 1999;41(4):303.
[52] Merz B, Bárdossy A. Effects of spatial variability on the rainfall runoff process in a small loess catchment. J Hydrol 1998;212–213:304–17.
[53] Steichen J. Infiltration and random roughness of a tilled and untilled claypan soil. Soil Till Res 1984;4(3):251–62.
[54] Mwendera E, Feyen J. Effects of tillage and rainfall on soil surface roughness and properties. Soil Technol 1994;7(1):93–103.
[55] Brent RP. Algorithm for minimization without derivatives. Englewood Cliffs, New Jersey: Prentice-Hall; 1973.
[56] Duan Q, Sorooshian S, Gupta V. Effective and efficient global optimization for conceptual rainfall-runoff models. Water Resour Res 1992;28(4):1015.
[57] Draper NR, Smith H. Applied regression analysis. 3rd ed. New York: John and Wiley and Sons; 1998.
[58] Nash J, Sutcliffe J. River flow forecasting through conceptual models part I – a discussion of principles. J Hydrol 1970;10(3):282–90.
[59] Krause P, Boyle DP, Bäse F. Comparison of different efficiency criteria for hydrological model assessment. Adv Geosci 2005;5:89–97.
[60] Robinson JS, Sivapalan M. Catchment-scale runoff generation model by aggregation and similarity analyses. Hydrol Process 1995;9(5-6):555–74.
[61] Viney NR, Sivapalan M. A framework for scaling of hydrologic conceptualizations based on a disaggregation–aggregation approach. Hydrol Process 2004;18(8):1395–408.
[62] Young PC, Ratto M. A unified approach to environmental systems modeling. Stoch Environ Res Risk Assess 2008;23(7):1037–57.